Chapter 3
Airborne MTI

James K. Day

Lockheed Martin Corporation

Fred M. Staudaher*

Naval Research Laboratory (retired)

3.1 SYSTEMS USING AIRBORNE MTI TECHNIQUES

Airborne search radars were initially developed for the detection of ships by long-range patrol aircraft. During the latter part of World War II, airborne early-warning (AEW) radars were developed by the U.S. Navy to detect low-flying aircraft approaching a task force below the radar coverage of the ship's antenna. The advantage of the airborne platform in extending the maximum detection range for air and surface targets is apparent when one considers that the radar horizon is 12 nmi for a 100-ft antenna mast compared with approximately 195 nmi for a 25,000-ft aircraft altitude.

The aircraft carrier–based E-2D aircraft (Figure 3.1) uses AEW radar as the primary sensor in its airborne tactical data system. These radars with their extensive field of view are required to detect small airborne targets against a background of sea and land clutter. Because their primary mission is to detect low-flying aircraft, they cannot elevate their antenna beam to eliminate the clutter. These considerations have led to the development of airborne MTI (AMTI)[1,2,3] radar systems similar to those used in surface radars,[1,4–6] discussed in the preceding chapter.

The mission requirements for an AEW radar drive the need for 360° azimuthal coverage and long-range detection capability. The 360° azimuthal coverage requirement is because the AEW radar system is generally required to provide the first detection of airborne targets, without any a priori knowledge of the location of these targets. AEW systems have generally been developed at lower frequencies—this can be understood by reviewing the surveillance radar range equation:

$$R_{\max} = \frac{P_a A_e \sigma_t}{(4\pi)\, kT_0 F_n L\, (S/N)_0} \frac{t_s}{\Omega} \tag{3.1}$$

* Sections 3.4 through 3.8 and 3.10 were taken primarily from the second edition of the *Radar Handbook*, Chapter 16, authored by Fred Staudaher, with revisions made by James Day. The remaining sections of the chapter were authored by James Day.

FIGURE 3.1 **E**-2D airborne early-warning (AEW) aircraft showing rotodome housing the antenna

where t_s is the scan time and Ω is the surveillance volume coverage requirement (product of the azimuth and elevation angles).

As long as the beamwidths of the radar (in azimuth and elevation) are smaller than the region to be surveilled, this equation is not directly dependent upon frequency. However, key parameters in this equation are dependent upon frequency. Particularly, propagation losses for low altitude targets and target RCS (for some target types) are generally advantageous for lower frequencies. The result is that AEW systems have been developed at UHF, L band, and S band frequencies.

Airborne MTI radar systems have also been utilized to acquire and track targets in interceptor fire control systems. In this application, the systems have to discriminate against clutter only in the vicinity of a prescribed target. This allows the system to be optimized at the range and angular sector where the target is located. MTI is also used to detect moving ground vehicles by reconnaissance and tactical fighter aircraft.

The environment of high platform altitude, mobility, and speed, coupled with restrictions on size, weight, and power consumption, present a unique set of problems to the designer of airborne MTI systems. This chapter will be devoted to considerations unique to the airborne environment.

3.2 COVERAGE CONSIDERATIONS

Search radars generally require 360° azimuthal coverage. This coverage is difficult to obtain on an aircraft since mounting an antenna in the clear presents major drag, stability, and structural problems. When extensive vertical coverage is required, the aircraft's planform and vertical stabilizer distort and shadow the antenna pattern. Analysis of tactical requirements may show that only a limited coverage sector is required. However, this sector usually has to be capable of being positioned over the full 360° relative to the aircraft's heading because of the requirements for coverage

FIGURE 3.2 Boeing 737-700 Wedgetail aircraft showing antennas mounted above the fuselage

while reversing course, large crab angles when high winds are encountered, the need to position ground track in relation to wind, nontypical operating situations, and operations requirements for coverage while proceeding to and from the station.

However, in the 1990s and 2000s, a number of systems have been developed that provide phased array performance in an airborne platform. The Multi-Role Electronically Scanned Array (MESA) radar developed by Northrop Grumman on a Boeing 737-700 for the Australian Wedgetail program is an example (see Figure 3.2). An alternate solution that combines mechanical scanning in conjunction with electronic scanning is in development with the AN/APY-9 radar for the E-2D aircraft (follow-up to the U.S. Navy's E-2C aircraft).

3.3 AIRBORNE MTI PERFORMANCE DRIVERS

The performance of airborne MTI systems are primarily determined by motion effects induced on the clutter echoes (platform motion, antenna scanning motion, and clutter internal motion), the processing techniques used to enhance target detection and maximize clutter cancellation, and the hardware stability limitations of the radar. This chapter will discuss the motion effects as well as the performance of various processing techniques.

3.4 PLATFORM MOTION AND ALTITUDE EFFECTS ON MTI PERFORMANCE

MTI discriminates between airborne moving targets and stationary land or sea clutter. However, in the airborne case, the clutter moves with respect to the moving airborne platform. It is possible to compensate for the mean clutter radial velocity by using

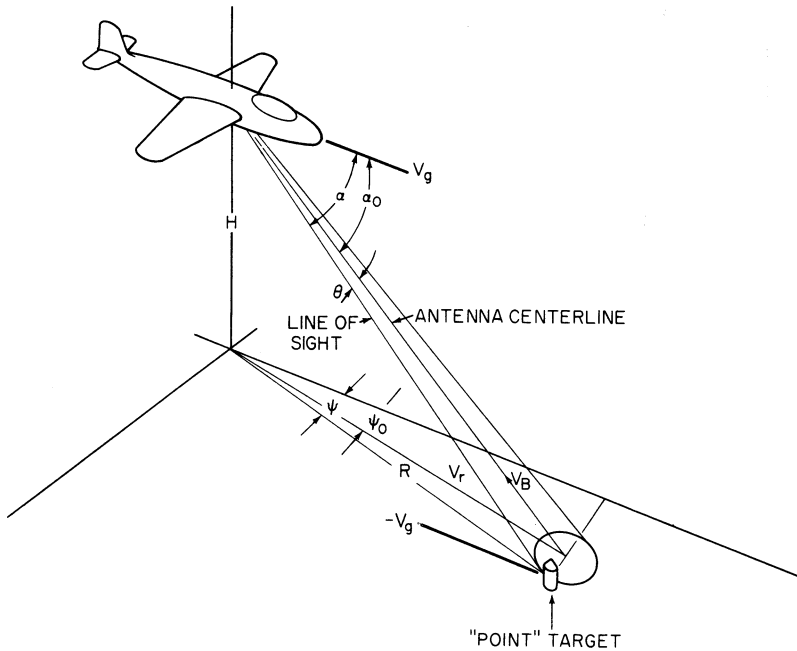

FIGURE 3.3 Defining geometry: α_0 = antenna pointing angle; α = line-of-sight angle; θ = angle from antenna centerline; V_g = aircraft ground speed; V_r = radial velocity of point target; V_B = radial velocity along antenna centerline (boresight); ψ_0 = antenna azimuth angle; ψ = azimuth angle; R = ground range to point target; and H = aircraft height

techniques such as time-averaged-clutter coherent airborne radar (TACCAR). This technique attempts to center the largest return from main-beam clutter at zero doppler frequency such that a simple MTI filter, also centered at zero doppler frequency, will cancel the main-beam clutter.

As shown in Figure 3.3, the apparent radial velocity of the clutter is $V_r = -V_g \cos \alpha$, where V_g is the ground speed of the platform and α is the angle subtended between the line-of-sight to a point on the Earth's surface and the aircraft's velocity vector. Figure 3.4 shows the loci of constant radial velocity along the surface. In order to normalize the figure, a flat earth is assumed, and the normalized radial velocity $V_n = V_r/V_g$ is presented as a function of azimuth angle ψ and normalized ground range R/H, where H is the aircraft's altitude.

Instead of a single clutter doppler frequency corresponding to a constant radial velocity (V_B in Figure 3.3) determined by the antenna pointing angle α_0, the radial sees a continuum of velocities. This results in a frequency spectrum at a particular range whose shape is determined by the antenna pattern that intersects the surface, the reflectivity of the clutter, and the velocity distribution within the beam. Furthermore, since V_r varies as a function of range at a particular azimuth ψ, the center frequency and spectrum shape vary as a function of range and azimuth angle ψ_0.

When the antenna is pointing ahead, the predominant effect is the variation of the center frequency corresponding to the change in α_0 with range. When the antenna is pointing

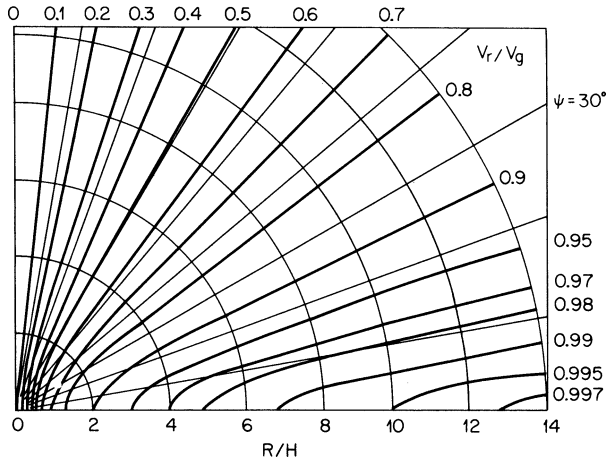

FIGURE 3.4 Loci of constant normalized radial velocity V_r/V_g as a function of aircraft range-to-height ratio R/H and azimuth angle ψ

abeam, the predominant effect is the velocity spread across the antenna beamwidth. These are classified as the slant-range effect and the platform-motion effect, respectively.

Effect of Slant Range on Doppler Offset. The antenna boresight velocity V_B is the ground-velocity component along the antenna centerline (boresight) and is given as $(-V_g \cos \alpha_0)$. If the clutter surface were coplanar with the aircraft, this component would be equal to $(-V_g \cos \psi_0)$ and would be independent of range. The ratio of the actual boresight velocity to the coplanar boresight velocity is defined as the normalized boresight-velocity ratio:

$$VBR = \frac{\cos \alpha_0}{\cos \psi_0} = \cos \phi_0 \tag{3.2}$$

where ϕ_0 is the depression angle of the antenna centerline from the horizontal. Figure 3.5 shows the variation of the normalized boresight-velocity ratio as a function of slant range for a curved earth and different aircraft altitudes. The variation is fairly rapid for slant ranges less than 15 nmi.

It is desirable to center the clutter spectrum in the notch (i.e., minimum-response region) of the AMTI filter in order to obtain maximum clutter rejection. This can be accomplished by offsetting the IF or RF frequency of the radar signal by an amount equal to the average doppler frequency of the clutter spectrum. Because the clutter center frequency varies with range and azimuth when the radar is moving, it is necessary for the filter notch to track the doppler-offset frequency, using an open- or closed-loop control system such as TACCAR, described below.

An example of a received clutter spectrum given an antenna response is shown in Figure 3.6*a*. The TACCAR frequency offset then shifts main-beam clutter to zero doppler, as shown in Figure 3.6*b*.

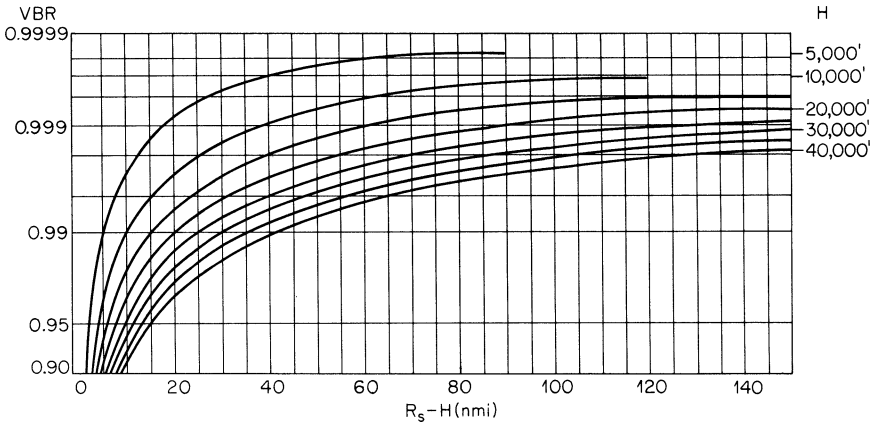

FIGURE 3.5 Normalized boresight-velocity ratio *VBR* as a function of the difference between slant range R_s and aircraft altitude H for different aircraft altitudes

TACCAR. The MIT Lincoln Laboratory originally developed TACCAR to solve the AMTI radar problem. The requirements and thus the implementation of TACCAR change depending upon the type of clutter cancellation processing employed. After many other approaches, it was recognized that if one used the clutter return rather than the transmit pulse to phase-lock the radar to the clutter filter, one could center the clutter in the filter stopband. The clutter phase varies from range cell to range cell owing to the distribution of the location of the scatterers in azimuth. Hence, it is necessary to average the return for as long an interval as possible. TACCAR is used to describe the centering of the returned clutter spectrum to the zero filter frequency. Since the technique compensates for drift in the various system elements and biases in the mean doppler frequency due to ocean currents, chaff, or weather clutter, it is used in shipboard and land-based radars as well as airborne radar.

A functional block diagram of an airborne radar employing TACCAR is shown in Figure 3.7. The clutter error signal is obtained by measuring the pulse-to-pulse phase shift $\omega_d T_p$ of the clutter return. This provides a very sensitive error signal. The averaged error signal controls a voltage-controlled coherent master oscillator (COMO), which determines the transmitted frequency of the radar. The COMO is slaved to

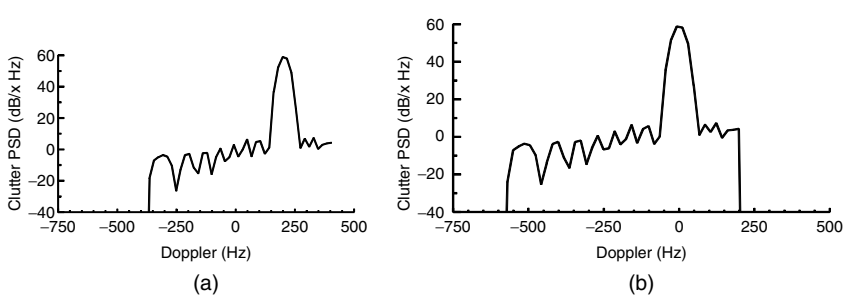

FIGURE 3.6 Clutter Power Spectral Density (PSD) response through antenna pattern: *a*) without TACCAR frequency offset and *b*) with TACCAR frequency offset

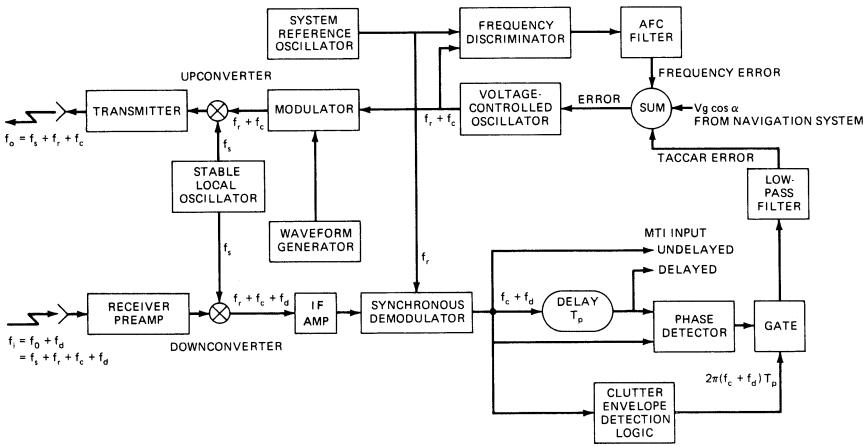

FIGURE 3.7 Block diagram of a radar illustrating the signal flow path of the TACCAR control loop

the system reference oscillator frequency via the automatic frequency control (AFC) loop shown in Figure 3.7. This provides a stable reference in the absence of clutter. An input from the aircraft inertial navigation system and the antenna servo provide a predicted doppler offset. These inputs allow the TACCAR system to provide a narrow-bandwidth correction signal.

Because of the noisy nature of the clutter signal, the need to have the control system bridge regions of weak clutter return, and the requirement not to respond to the doppler shift of a true target, the control system usually tracks the azimuth variation of a specific radar range interval. The maximum range of this interval is chosen so that clutter will be the dominant signal within the interval. The minimum range is chosen to exclude signals whose average frequency differs substantially from the frequency in the region of interest.

Alternate approaches to providing this frequency offset can be implemented with digital exciters or on receive. For some applications, it may be necessary to use multiple control loops, each one covering a specific range interval, or to vary the offset frequency in range. This is possible if the frequency offset is implemented on receive (but not on transmit). At any particular range, the filter notch is effectively at one frequency and the center frequency of the clutter spectrum at another. The difference between these frequencies results in a doppler-offset error, as shown in Figure 3.8. The clutter spectrum will extend into more of the filter passband, and the clutter improvement factor will be degraded. The required accuracy for the TACCAR control loop can be relaxed if the MTI filter is an adaptive filter, such as with space-time adaptive processing (discussed later in this chapter). This is because the adaptive filter will adjust to the received signals and optimize clutter cancellation.

Without adaptive adjustment, Figure 3.9 shows the improvement factor for single- and double-delay cancelers as a function of the ratio of the notch-offset error to the pulse repetition frequency (PRF) for different clutter spectral widths. Fortunately, the platform-motion spectrum is narrow in the forward sector of coverage where offset error is maximum. An offset error of one-hundredth of the PRF would yield a 26 dB improvement factor for a double canceler with an input clutter spectrum whose width

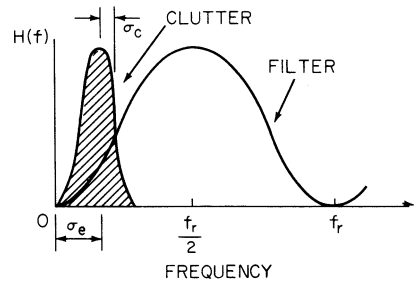

FIGURE 3.8 Effect of doppler-offset error; f_r = PRF

was 3% of the PRF. If the radar frequency were 10 GHz, PRF 1 kHz, and ground speed 580 kt, the notch would have to be held within 0.29 kt or $0.005V_g$.

Because of these requirements and the width of the platform-motion spectrum, stagger PRF systems must be chosen primarily on the basis of maintaining the stopband rather than flattening the passband. Similarly, higher-order delay-line filters (with or without feedback) are synthesized on the basis of stopband rejection. The limiting case is the narrowband filter bank where each individual filter consists of a small passband, the balance being stopband.

Improvement factor is an important metric, but in addition to this average metric defined across all doppler frequencies, it is often important to characterize the performance as a function of doppler frequency, particularly with coherent doppler filtering imbedded in the processing chain. With performance characterized versus doppler

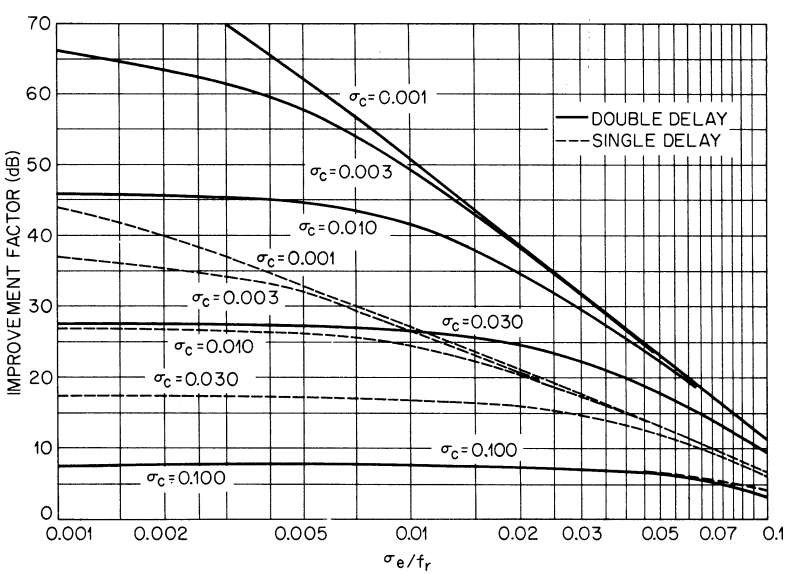

FIGURE 3.9 Improvement factor I versus normalized doppler offset σ_e as a function of clutter spectrum width σ_c

frequency, the radar design can then be evaluated through the complete detection chain and optimized in conjunction with any multiple PRF stagger waveforms utilized to bridge MTI blind regions.

Platform-Motion Effect. To an airborne radar, a clutter scatterer appears to have a radial velocity that differs from the antenna-boresight radial velocity at the same range by

$$\begin{aligned} V_e &= V_r - V_B \\ &= V_g \cos\alpha_0 - V_g \cos\alpha \\ &= V_g[\cos\alpha_0 - \cos(\alpha_0 + \theta)] \\ &= V_x \sin\theta + 2V_y \sin^2\frac{\theta}{2} \end{aligned} \tag{3.3}$$

for small values of θ and depression angle ϕ_0, where V_x is the horizontal component of velocity perpendicular to the antenna boresight and V_y is the component along the antenna boresight. θ is the azimuthal angle from the antenna boresight, or the intersection of the vertical plane containing the boresight with the ground. The corresponding doppler frequency, when α_0 is a few beamwidths from ground track, is

$$f_d = \frac{2V_x}{\lambda}\sin\theta \approx \frac{2V_x}{\lambda}\theta \tag{3.4}$$

This phenomenon results in a platform-motion clutter power spectrum that is weighted by the antenna's two-way power pattern in azimuth. The true spectrum may be approximated by a gaussian spectrum,

$$H(f) = e^{-\frac{1}{2}\left(f_d/\sigma_{\text{pm}}\right)^2} = e^{-2\left(V_x\theta/\lambda\sigma_{\text{pm}}\right)^2} \approx G^4(\theta) \tag{3.5}$$

$G^4(\theta)$, the two-way power pattern of the antenna, is 0.25 when $\theta = \theta_a/2$, where θ_a is the half-power beamwidth, which can be approximated by λ/a, a being the effective horizontal aperture width. Thus,

$$e^{-\frac{1}{2}\left(V_x/a\sigma_{\text{pm}}\right)^2} = 0.25$$

or

$$\sigma_{\text{pm}} = 0.6\frac{V_x}{a} \tag{3.6}$$

where V_x and a are in consistent units. This value is lower than ones derived by other authors.[4,5] However, it agrees with more exact analysis of antenna radiation patterns and experimental data analyzed by F. Staudaher.

A more exact value of the parameter σ_{pm} may be obtained by matching a two-way power pattern of interest with the gaussian approximation at a specific point on the pattern, determining the standard deviation of θ by using statistical techniques or fitting

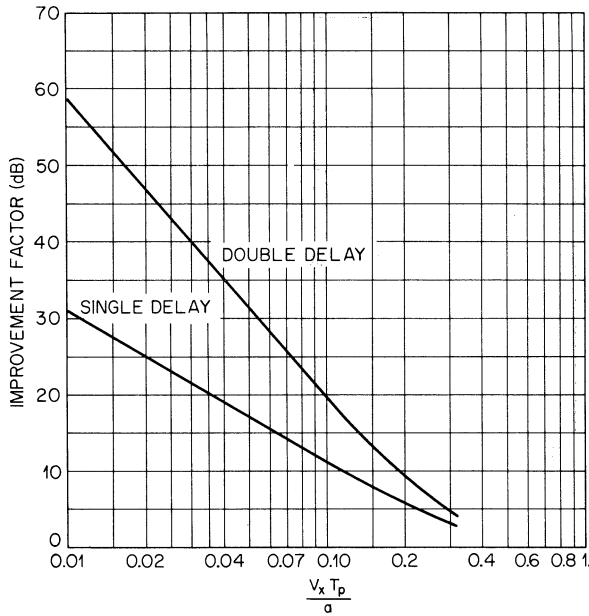

FIGURE 3.10 Effect of platform motion on the MTI improvement factor as a function of the fraction of the horizontal antenna aperture displaced per interpulse period, $V_x T_p/a$

the pattern and using numerical methods. The calculation of the improvement factor can be performed by averaging the resultant residue power, obtained by summing the signal phasors at specific values of θ, from null to null of the antenna pattern.

Figure 3.10 shows the effect of platform motion on the MTI improvement factor as a function of the aperture displaced in the plane of the aperture per interpulse period T_p. A 5.4% displacement reduces the double-delay improvement factor to 30 dB. This corresponds to a speed of 325 kt if the system has a PRF of 1000 Hz and a 10-ft antenna aperture. For a single-delay system, the displacement has to be held to 1.1% for a 30 dB performance limit.

3.5 PLATFORM-MOTION COMPENSATION ABEAM

The deleterious effects of platform motion can be reduced by physically or electronically displacing the antenna phase center along the plane of the aperture. This is referred to as the *displaced phase center antenna (DPCA) technique*.[7–11] In addition, some forms of space-time adaptive processing are expressly developed to improve clutter cancellation with an adaptive filter, electronically displacing the antenna phase center.

Electronically Displaced Phase Center Antenna. Figure 3.11*a* shows the pulse-to-pulse phase advance of an elemental scatterer as seen by the radar receiver.

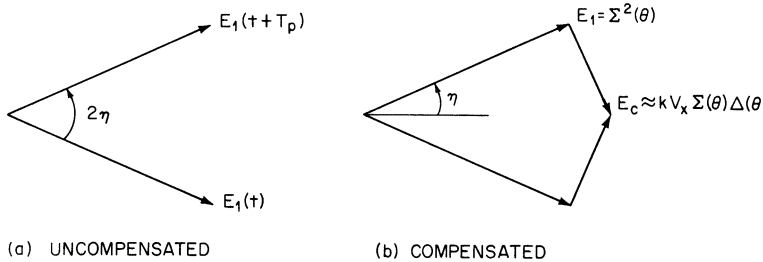

FIGURE 3.11 Phasor diagram showing the return from a point scatterer due to platform motion

The amplitude E_1 of the received signal is proportional to the two-way antenna field intensity. The phase advance is

$$2\eta = 2\pi f_d T_p = \frac{4\pi V_x T_p \sin\theta}{\lambda} \tag{3.7}$$

where f_d = doppler shift of scatterer (Eq. 3.4)
T_p = interpulse period

Figure 3.11*b* shows a method of correcting for the phase advance η. An idealized correction signal E_c is applied, leading the received signal by 90° and lagging the next received signal by 90°. For exact compensation, the following relation would hold:

$$E_c = E_1 \tan\eta = \Sigma^2(\theta)\tan\frac{2\pi V_x T_p \sin\theta}{\lambda} \tag{3.8}$$

This assumes a two-lobe antenna pattern similar to that in a monopulse tracking radar. Two receivers are used, one supplying a sum signal, $\Sigma(\theta)$, and the other a difference signal, $\Delta(\theta)$. The difference signal is used to compensate for the effects of platform motion.

If the system is designed to transmit the sum pattern $\Sigma(\theta)$ and receive both $\Sigma(\theta)$ and a difference pattern $\Delta(\theta)$, then at the design speed the received signal $\Sigma(\theta)\Delta(\theta)$ can be applied as the correction signal. The actual correction signal used to approximate E_c is $k\,\Sigma(\theta)\Delta(\theta)$, where k is the ratio of the amplification in the sum and difference channels of the receiver.

A uniformly illuminated monopulse array[12] has the difference signal Δ in quadrature with the sum and has the amplitude relationship

$$\Delta(\theta) = \Sigma(\theta)\tan\left(\frac{\pi W}{\lambda}\sin\theta\right) \tag{3.9}$$

where W is the distance between the phase centers of the two halves of the antenna. Hence, a choice of $W = 2V_xT_p$ and $k = 1$ would ideally result in perfect cancellation.

In practice, a sum pattern is chosen based on the desired beamwidth, gain, and sidelobes for the detection system requirements. Then the difference pattern $\Delta(\theta)$ is synthesized independently, based on the relationship required at design radar platform

speed and allowable sidelobes. The two patterns may be realized by combining the elements in separate corporate-feed structures.

Figure 3.12 shows the idealized improvement factor as a function of normalized aperture movement for a double-delay canceler. The improvement factor shown is the improvement factor for a point scatterer averaged over the null-to-null antenna beamwidth. In one case, the gain ratio k is optimized at each value of pulse-to-pulse displacement. In the other compensated case, the optimum gain ratio k is approximated by the linear function of interpulse platform motion kV_x.

A block diagram of the double-delay system is shown in Figure 3.13. A single-delay system would not have the second delay line and subtractor. The normally required circuitry for maintaining coherence, gain and phase balance, and timing is not shown. The speed control V_x is bipolar and must be capable of reversing the sign of the $\Delta(\theta)$ signal in each channel when the antenna pointing angle changes from the port to the starboard side of the aircraft.

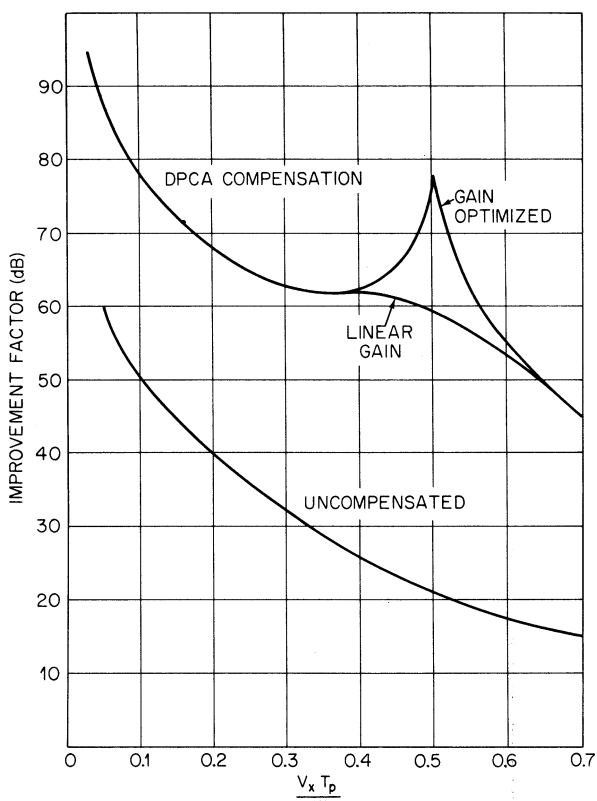

FIGURE 3.12 MTI improvement factor for DPCA compensation as a function of the fraction of the horizontal phase center separation W that the horizontal antenna aperture is displaced per interpulse period, V_xT_p/W. $W = 0.172a$, where a is the horizontal aperture length.

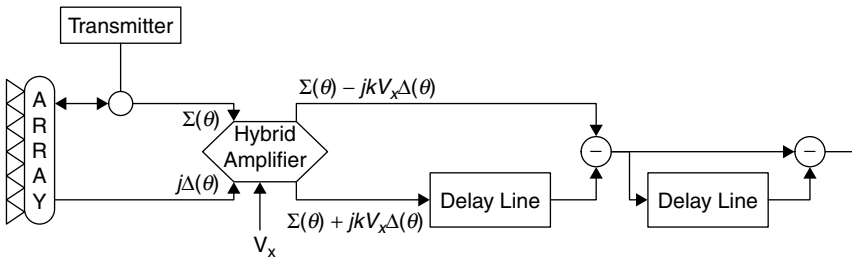

FIGURE 3.13 Simplified double-delay DPCA mechanization

The hybrid amplifier shown has two input terminals that receive $\Sigma(\theta)$ and $j\Delta(\theta)$ and amplify the $\Delta(\theta)$ channel by kV_x relative to the $\Sigma(\theta)$ channel. The output terminals produce the sum and difference of the two amplified input signals. Because DPCA compensates for the complex signal, both amplitude and phase information must be retained. Therefore, these operations usually occur at RF or IF. Digital compensation can be used if synchronous detection and analog to digital (A/D) conversion are performed and the components are treated as complex phasors. Furthermore, the operations must be linear until the sum signal and difference signals have been processed by the hybrid amplifier. After this single-pulse combination, the actual double cancellation can be performed by any conventional MTI processing techniques.

Power in the Antenna Sidelobes. Airborne systems are limited in their ability to reject clutter due to the power returned by the antenna sidelobes. The full 360° azimuthal pattern sees velocities from $-V_g$ to $+V_g$. The compensation circuits offset the velocity by an amount corresponding to the antenna boresight velocity V_B, but the total range of doppler frequencies corresponding to $2V_g$ is obtained because of echoes received via the sidelobes. For airborne systems with low PRFs, these doppler frequencies can cover several multiples of the PRF so that the sidelobe power is folded into the filter. This limitation is a function of the antenna pointing angle, the MTI filter response, and the sidelobe pattern. If the sidelobes are relatively well distributed in azimuth, a measure of performance can be obtained by averaging the power returned by the sidelobes.

The limiting improvement factor due to sidelobes is

$$I_{\text{sl limit}} = \frac{K\int_{-\pi}^{\pi} G^4(\theta)\,d\theta}{\int_{\text{sl}} G^4(\theta)\,d\theta} \tag{3.10}$$

where the lower integral is taken outside the main-beam region. Main-beam effects would be included in the platform-motion improvement factor. The constant K is the noise normalization factor for the MTI filter ($K = 2$ for single delay and 6 for double delay.) $G^4(\theta)$ is the two-way power of the antenna in the plane of the ground surface.

The DPCA performance described in the preceding subsection can be analyzed on the basis of radiation patterns or the equivalent aperture distribution function.[8] If the radiation pattern is used, the composite performance may be obtained either by applying the pattern functions over the entire 360° pattern or by combining the improvement

factors for the DPCA main-beam and the sidelobe regions in the same manner as parallel impedances are combined:

$$\frac{1}{I_{\text{total}}} = \frac{1}{I_{sl}} + \frac{1}{I_{\text{DPCA}}} \tag{3.11}$$

If the aperture distribution is used, the sidelobe effects are inherent in the analysis. Care must be taken, however—if the array or reflector function is used without considering the weighting of the elemental pattern or the feed distribution, the inherent sidelobe pattern can obscure the main-beam compensation results.

Again, the performance versus doppler frequency is important for evaluating overall radar detection performance. Antenna sidelobe limited performance can be approximated by performing the lower integral of Eq. 3.10 over those angles that map into a given doppler filter's passband. The noise normalization term, k, must also be modified to reflect the cascaded noise gain of the MTI and doppler filter bank as

$$N_g(k) = 6\sum_{i=1}^{N} W_i^2 - 8\sum_{i=1}^{N-1} W_i W_{i+1}\cos(2\pi k/N) + 2\sum_{i=1}^{N-2} W_i W_{i+2}\cos(4\pi k/N); \quad k = 0, N-1 \tag{3.12}$$

for three-pulse MTI and cascaded N-pulse doppler filter bank, where W_i are the doppler filter weights, or

$$N_g(k) = 2\sum_{i=1}^{N} W_i^2 - 2\sum_{i=1}^{N-1} W_i W_{i+1}\cos(\pi k/N); \quad k = 0, N-1 \tag{3.13}$$

for two-pulse MTI and cascaded N-pulse doppler filter bank.

3.6 SCANNING-MOTION COMPENSATION

Figure 3.14*a* shows a typical antenna main-beam radiation pattern and the response of a point scatterer for two successive pulses when the antenna is scanning. It is seen that the signals returned would differ by $\Delta G^2(\theta)$. This results in imperfect cancellation due to scanning. The average effect on the improvement factor can be obtained by integrating this differential effect $\Delta G^2(\theta)$ over the main beams:

$$I_{\text{scan}} = \frac{2\int_{-\theta_0}^{\theta_0} |G(\theta)|^2\, d\theta}{\int_{-\theta_0}^{\theta_0} |G(\theta + T_p\dot{\theta}) - G(\theta)|^2\, d\theta} \quad \text{for single-delay cancellation} \tag{3.14a}$$

$$I_{\text{scan}} = \frac{6\int_{-\theta_0}^{\theta_0} |G(\theta)|^2\, d\theta}{\int_{-\theta_0}^{\theta_0} |G(\theta + T_p\dot{\theta}) - 2G(\theta) + G(\theta - T_p\dot{\theta})|^2\, d\theta} \quad \text{for double-delay cancellation} \tag{3.14b}$$

where θ_0 = null of main beam
$G(\theta)$ = two-way voltage pattern

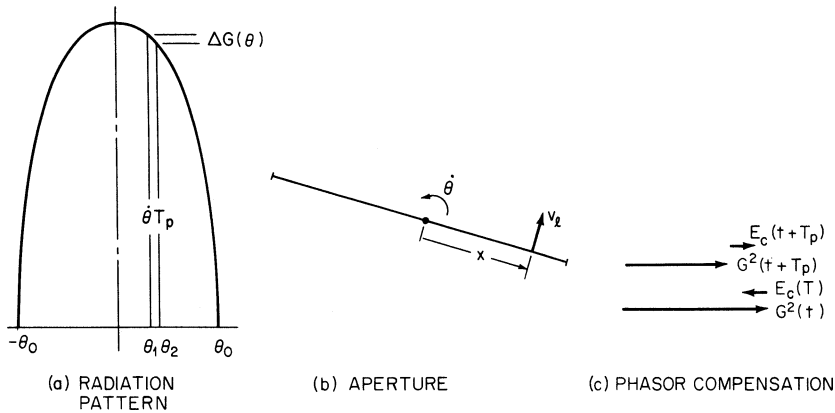

FIGURE 3.14 Antenna scanning effects: (*a*) as seen by the antenna radiation pattern, due to the apparent change in azimuth of the scatterer, $\theta_2 - \theta_1 = \dot{\theta}\, T_p$; (*b*) as seen by the aperture illumination function, due to the apparent motion, $v_1 = x\dot{\theta}$, of the scatterer relative to the antenna at position x; and (*c*) step-scan compensation of two received phasors

In order to treat scanning motion in the frequency domain, the apparent clutter velocity seen by the scanning antenna is examined to determine the doppler frequency. Each element of an array or incremental section of a continuous aperture can be considered as receiving a doppler-shifted signal due to the relative motion of the clutter. The power received by the element is proportional to the two-way aperture power distribution function $F_2(x)$ at the element.

In addition to the velocity seen by all elements because of the motion of the platform, each element sees an apparent clutter velocity due to its rotational motion, as illustrated in Figure 3.14*b*. The apparent velocity varies linearly along the aperture. Hence, the two-way aperture distribution is mapped into the frequency domain. The resulting power spectrum due to the antenna scanning is

$$H(f) = F_2\left(\frac{\lambda f}{2\dot{\theta}}\right) \qquad 0 \le f \le \frac{a\dot{\theta}}{\lambda} \tag{3.15}$$

where $\dot{\theta}$ = antenna rotation rate
a = horizontal antenna aperture

This spectrum can be approximated by a gaussian distribution with standard deviation

$$\sigma_c = 0.265\frac{f_r}{n} = 0.265\frac{\dot{\theta}}{\theta_a} \approx 0.265\frac{a\dot{\theta}}{\lambda} \tag{3.16}$$

where λ and a are in the same units, θ_a is the one-way half-power beamwidth, and n is the number of hits per beamwidth. The approximation $\theta_a \approx \lambda/a$ is representative of an antenna distribution yielding acceptable sidelobe levels.

It can be seen that the antenna pattern pulse-to-pulse differential gain is

$$\Delta G^2(\theta) = \frac{dG^2(\theta)}{d\theta}\Delta\theta = \frac{dG^2(\theta)}{d\theta}\dot{\theta}T_p \tag{3.17}$$

This suggests[7,13] that a correction signal in the reverse sense to $\Delta G^2(\theta)$ be applied, as shown in Figure 3.14*c*. Half the correction is added to one pulse and half subtracted from the other, so that

$$\begin{aligned}\text{Correction signal} &= \frac{\Delta G^2(\theta)}{2} = \frac{\dot{\theta} T_p}{2} \frac{d\Sigma^2(\theta)}{d\theta} \\ &= \dot{\theta} T_p \Sigma(\theta) \frac{d\Sigma(\theta)}{d\theta}\end{aligned} \tag{3.18}$$

where $\Sigma^2(\theta)$ was substituted for $G^2(\theta)$. The radar transmits a sum pattern $\Sigma(\theta)$ and receives on the difference pattern $\Delta(\theta)$, so that the received signal is proportional to the product of the two. If the signal received on the difference pattern is used as the correction, we have

$$E_c = \Delta(\theta)\Sigma(\theta) \tag{3.19}$$

By comparing Eqs. 3.18 and 3.19, we see that for E_c to approximate the correction signal, the difference patterns should be

$$\Delta(\theta) = \dot{\theta} T_p \frac{d\Sigma(\theta)}{d\theta} \tag{3.20}$$

The derivative of the sum pattern is similar to a difference pattern in that it is positive at the main-beam null, $-\theta_0$, decreases to zero on the antenna centerline, and then goes negative until θ_0.

Referring to Figure 3.13, one observes that the mechanization for scan compensation is fundamentally similar to the DPCA mechanization except that the difference signal is applied in phase with the sum signal and amplified by an amount determined by the antenna rotation per interpulse period.

The signals required, if the transmission signal $\Sigma(\theta)$ that appears in each channel is neglected, are $\Sigma(\theta) \pm l\dot{\theta} T_p \Delta(\theta)$, where l is the ratio of the amplification in the two channels chosen to maximize the clutter rejection. The required difference-pattern slope is determined by the derivative of the scan pattern, which differs from the DPCA criterion. This technique is known as *step-scan compensation* because the system electronically points the antenna slightly ahead of and behind of boresight each pulse so that a leading and lagging pair are taken from successive returns to obtain the effect of the antenna remaining stationary.

Figure 3.15 shows the improvement obtained by Dickey and Santa[7] for single-delay cancellation.

Compensation-Pattern Selection. Selection of the compensation pattern depends on the level of system performance required, the type of MTI filtering used, the platform velocity, scan rate, and the characteristics required by normal radar parameters such as resolution, distortion, gain, sidelobes, etc. For instance, an exponential pattern and its corresponding difference pattern are excellent for single-delay-cancellation DPCA but are unsatisfactory when double-delay cancellation is used. This is because the single-delay canceler requires the best match between the actual pattern and the required pattern near boresight, whereas double cancellation requires the best match

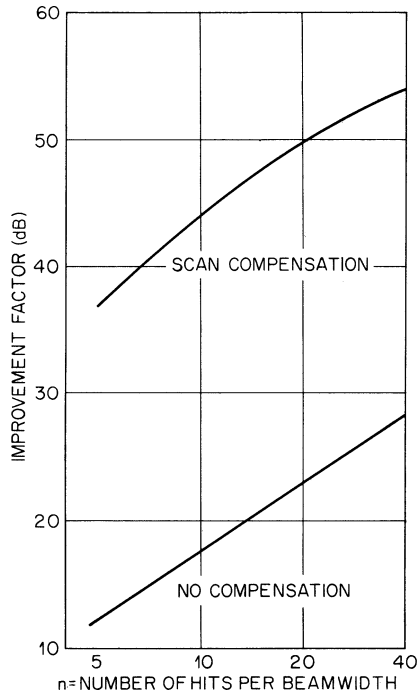

FIGURE 3.15 MTI improvement factor for a step-scan compensation of a single-delay canceler as a function of the number of hits per beamwidth. The antenna pattern is $(\sin x)/x$.

on the beam shoulder. Step-scan compensation usually requires the difference-pattern peaks to be near the nulls of the sum pattern to match.

Grissetti et al.[13] have shown that for step-scan compensation the improvement factor for single-delay cancellation increases as a function of the number of hits at 20 dB/decade; for the first-derivative*-type step-scan compensation, at the rate of 40 dB/decade; and with first- and second-derivative compensation, at the rate of 60 dB/decade. Hence, for a ground-based system that is limited by scan rate, one should improve the compensation pattern rather than use a higher-order MTI canceler. However, airborne systems are primarily limited by platform motion and require both better cancelers and compensation for operation in a land-clutter environment. In the sea-clutter environment, the system is usually dominated by the spectral width of the velocity spectrum or platform motion rather than scanning. The applicability of DPCA or step-scan compensation in the latter case is dependent on the particular system parameters.

* The compensation required by $\Delta G^2(\theta)/2$ can be determined from a Taylor's series expansion of $G^2(\theta)$. In the preceding discussion, we used the first derivative. Using higher-order terms gives an improved correction signal.

3.7 SIMULTANEOUS PLATFORM MOTION AND SCAN COMPENSATION

In AMTI systems having many hits per scan, scanning is a secondary limitation for an uncompensated double canceler. However, the performance of a DPCA system is significantly reduced when it is scanned. This is due to the scanning modulation on the difference pattern used for platform-motion compensation.

Since the DPCA applies the difference pattern in quadrature to the sum pattern to compensate for phase error and step scan applies the difference pattern in phase to compensate for amplitude error, it is possible to combine the two techniques by properly scaling and applying the difference pattern both in phase and in quadrature. The scaling factors are chosen to maximize the improvement factor under conditions of scanning and platform motion.

The relationships for a double-delay (three-pulse) AMTI are shown in the phasor diagram in Figure 3.16. The phase advance between the first pair of pulses (first and second pulse for the three-pulse MTI) received by the sum pattern Σ is

$$2\eta_1 = \frac{4\pi T_p}{\lambda}\left[V_x\left(\sin\theta_2 - \sin\frac{\omega_r T_p}{2}\right) + V_y\left(\cos\frac{\omega_r Tp}{2} - \cos\theta_2\right)\right] \tag{3.21}$$

and the phase advance between the second pair of pulses (second and third pulse for the three-pulse MTI) is

$$2\eta_2 = \frac{4\pi T_p}{\lambda}\left[V_x\left(\sin\theta_2 + \sin\frac{\omega_r T_p}{2}\right) + V_y\left(\cos\frac{\omega_r Tp}{2} - \cos\theta_2\right)\right] \tag{3.22}$$

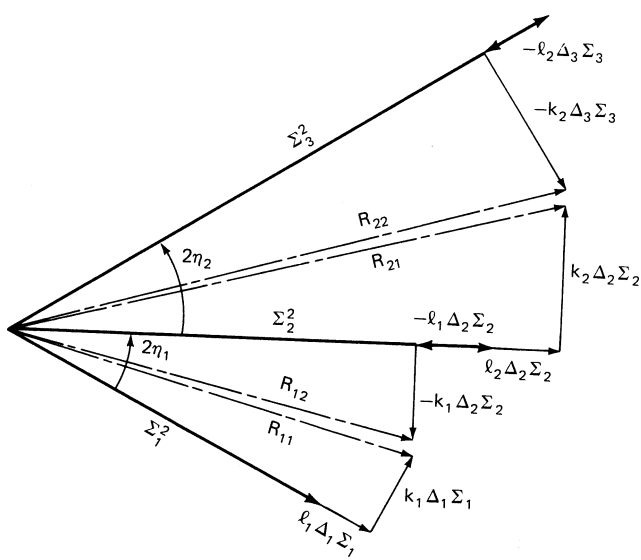

FIGURE 3.16 Phasor diagram for simultaneous scanning and motion compensation

where θ_2 is the direction of the clutter cell with respect to the antenna pointing angle when the second pulse is received and ω_r is the antenna scan rate. The subscripts on the received signals Σ_i and Δ_i indicate the pulse reception sequence.

The difference pattern Δ is used to generate an in-phase correction for scanning motion and a quadrature correction for platform motion. This process yields the set of resultant signals R_{ij}, where the subscript i denotes the pulse pair and the subscript j denotes the component of the pair. Because η_1 does not equal η_2, different weighting constants are required for each pulse pair. The values of k_1 for the quadrature correction of the first pulse pair, k_2 for the quadrature correction for the second pulse pair, l_1 for the in-phase correction for the first pulse pair, and l_2 for the second pulse pair are optimized by minimizing the integrated residue power over the significant portion of the antenna pattern, usually chosen between the first nulls of the main beam.

Figure 3.17 shows the sum and difference main-beam patterns for an aperture 20 wavelengths long. Figure 3.18 shows the residue for the case when the fraction of the horizontal aperture width a traveled per interpulse period T_p, $V_n = V_x T_p/a$, is equal to 0.04 and when the number of wavelengths that the aperture tip rotates per interpulse period, $W_n = a\omega_r T_p/2\lambda$, is equal to 0.04. The corresponding improvement factor is 52 dB.

The improvement factor is shown in Figure 3.19 for a range of normalized platform motion V_n as a function of normalized scanning displacements W_n. The nonscanning case is shown as $W_n = 0$. The improvement factors were computed for the 20-wavelength aperture patterns shown in Figure 3.17.

Andrews[14] has developed an optimization procedure for platform-motion compensation that rotates the phasors directly rather than by using a quadrature correction. The procedure determines the antenna feed coefficients for two compensation patterns, one of which, $C_1(\theta)$, is added to the sum pattern $\Sigma(\theta)$ and fed to the undelayed canceler

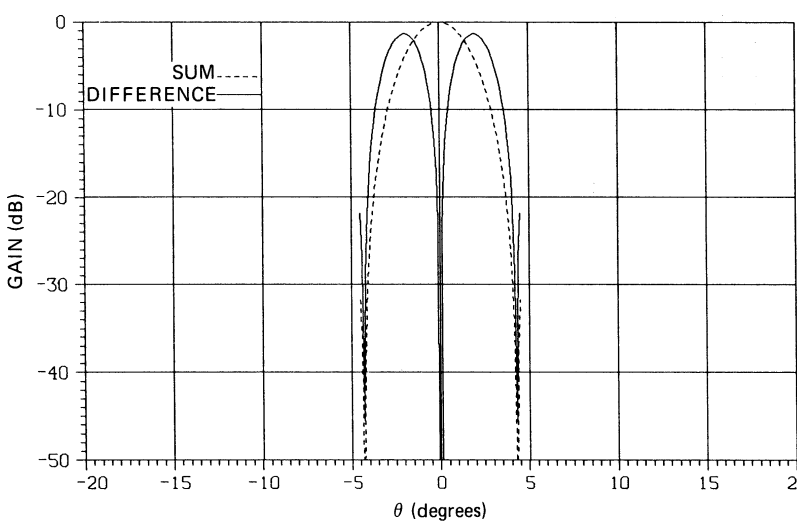

FIGURE 3.17 Sum and difference patterns used to determine DPCA performance

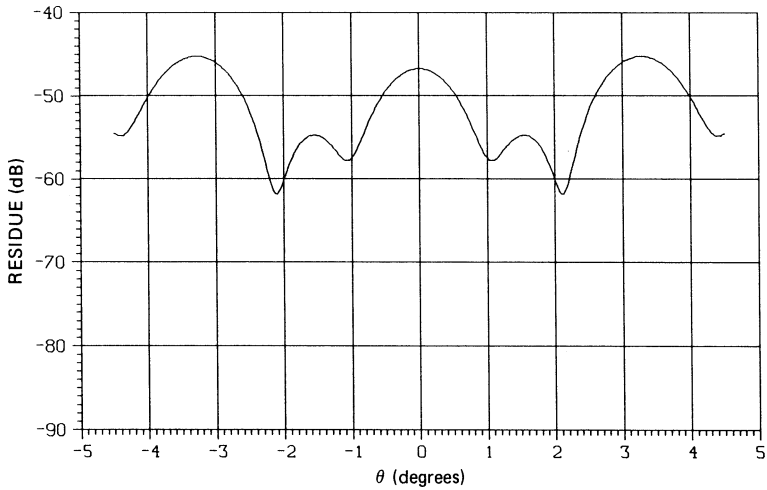

FIGURE 3.18 DPCA clutter residue versus angle for normalized displacement, $V_n = 0.04$, and normalized scanning motion, $W_n = 0.04$

path, and the other, $C_2(\theta)$, which is added to the sum pattern and fed to the delayed path as shown in Figure 3.20. The procedure was developed for a single-delay canceler and a nonscanning antenna. Andrews used the procedure to minimize the residue power over the full antenna pattern, which includes the main-beam and sidelobe regions.

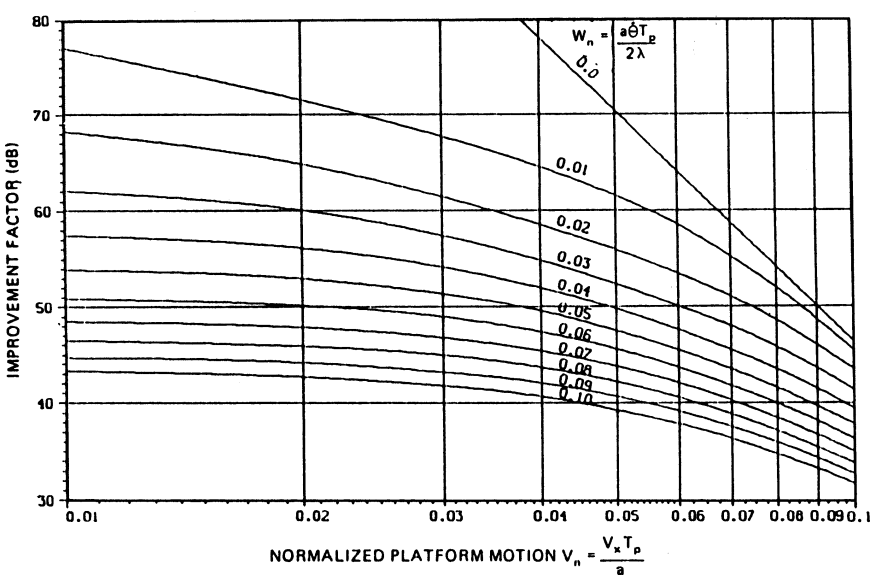

FIGURE 3.19 DPCA improvement factor versus normalized platform motion, V_n, as a function of normalized scanning motion, W_n

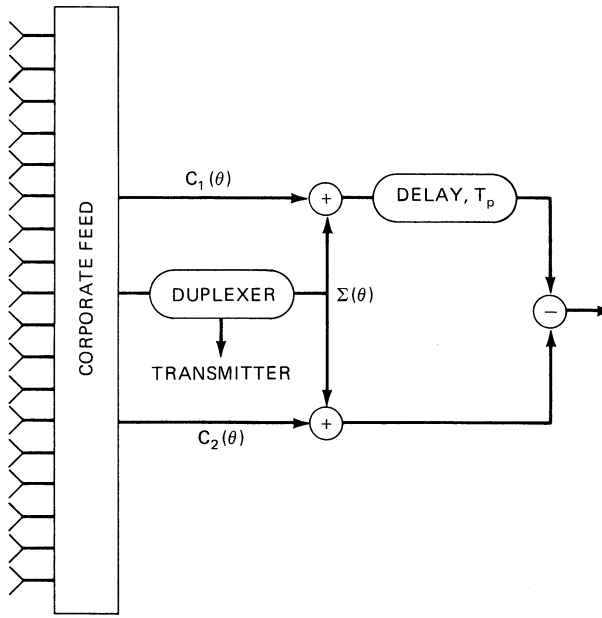

FIGURE 3.20 Optimized DPCA phase compensation

3.8 PLATFORM-MOTION COMPENSATION, FORWARD DIRECTION

The previous sections discussed the compensation for the component of platform motion parallel to the antenna aperture. TACCAR removes the average component of platform motion perpendicular to the aperture. The former Wheeler Laboratories developed the Coincident Phase Center Technique (CPCT)[15] to remove the spectral spread due to the velocity component perpendicular to the aperture and due to the component parallel to the aperture. Removal of the component parallel to the aperture uses the DPCA pattern synthesis technique described in Anderson,[8] which creates two similarly shaped illumination functions whose phase centers are physically displaced. Removal of the component perpendicular to the aperture is accomplished by a novel extension of this concept.

The first term of Eq. 3.3 for spectral width due to platform motion approaches zero as the antenna points ahead. However the second term of Eq. 3.3 dominates as the antenna approaches within a few beamwidths of the aircraft's ground track. In this region

$$f_d \approx \frac{4V_y}{\lambda} \sin 2\frac{\theta}{2} \approx \frac{V_y\theta^2}{\lambda} \tag{3.23}$$

which yields a single-sided spectrum that is significantly narrower than the spectrum abeam. For moderate platform speeds and lower-frequency (UHF) radars, this effect is negligible, and compensation is not required.

When it is necessary to compensate for this effect, the phase center of the antenna must be displaced ahead of the aperture and behind the aperture for alternate receive pulses so that the phase centers are coincident for a moving platform. This technique can be extended to more than two pulses by using the necessary phase-center displacements for each pulse. In order to maintain the effective PRF, the displacement must compensate for the two-way transmission path. To accomplish this displacement, near-field antenna principles are utilized. A desired aperture distribution function is specified. The near-field amplitude and phase are calculated at a given distance from the origin. If this field is used as the actual illumination function, a virtual aperture is created with the desired distribution function at the same distance behind the physical antenna. Figure 3.21*a*[15] shows the phase and amplitude distribution required to form a uniform virtual distribution displaced behind the physical aperture. It can be shown that if the phase of the illumination function is reversed $\phi' = -\phi$, the desired virtual distribution function is displaced ahead of the aperture, as shown in Figure 3.21*b*.

In practice, performance is limited by the ability to produce the required illumination function. As the displacement increases, a larger physical aperture size is required to produce the desired virtual aperture size owing to beam spreading. This can be seen in Figure 3.21. The effectiveness of the correction varies with elevation angle since the

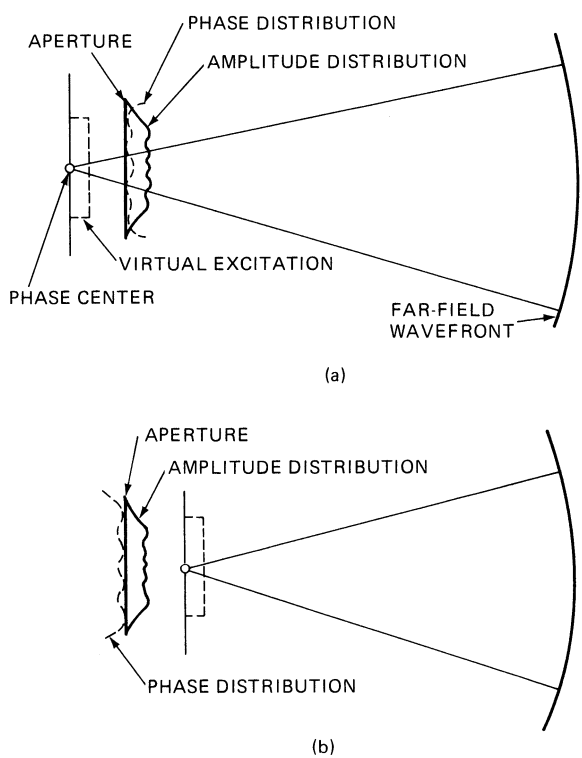

FIGURE 3.21 CPCT concept showing displacement of the phase center: (*a*) behind the physical aperture and (*b*) ahead of the physical aperture (*Courtesy of Hazeltine Inc.*[15])

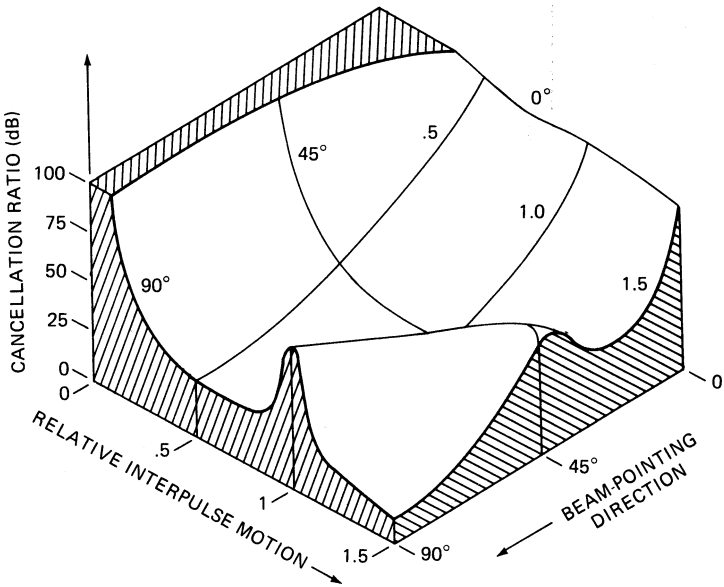

FIGURE 3.22 CPCT cancellation ratio, in decibels, as a function of relative interpulse motion and beam-pointing direction (*Courtesy of Hazeltine Inc.*[15])

actual displacement along the line-of-slight varies with elevation angle. This effect is more pronounced at higher aircraft speeds and higher radar frequencies. A change in the magnitude of the correction factor or even the compensation pattern with range, height, and velocity could be utilized to retain performance.

Figure 3.22 illustrates the theoretical MTI performance of a CPCT system as a function of beam-pointing direction and interpulse motion normalized to the interpulse motion used to design the compensation pattern. (*Cancellation ratio* is defined as the ratio of input clutter power to output clutter residue power.) The peak on the 90° axis is typical of the optimized DPCA performance illustrated in Figure 3.12.

3.9 SPACE-TIME ADAPTIVE MOTION COMPENSATION

Introduction. Several methods have been described to compensate for antenna motion. All these techniques are applied in the radar design phase for a specific set of operational parameters. Controls (usually automatic) are provided to adjust weights for operational conditions around the design value.

The development of digital radar technology and economical high-speed processors allows the use of dynamic space-time adaptive array processing (STAP),[16] whereby a set of antenna patterns that displace the phase center of the array both along and orthogonal to the array are continually synthesized to maximize the signal-to-clutter ratio. *Spatial adaptive array* processing combines an array of signals received at the same instant of time that are sampled at the different spatial locations corresponding

to the antenna elements. *Temporal adaptive array* processing combines an array of signals received at the same spatial location (e.g., the output of a reflector antenna) that are sampled at different instances of time, such as several interpulse periods for an adaptive MTI. Space-time adaptive array processing combines a two-dimensional array of signals sampled at different instances of time and at different spatial locations. STAP is a fairly broad topic that has applicability beyond this chapter on airborne MTI radar. The primary motivation for STAP is to improve clutter cancellation performance and to better integrate a radar's spatial processing (antenna sidelobe control and sidelobe jamming cancellation) with its temporal clutter cancellation processing.

The applicability of STAP to improving clutter cancellation must be assessed specifically in the context of the key performance limiters to airborne MTI radar clutter cancellation as described at the start of this chapter. STAP can improve a radar's motion compensation performance and is more robust than nonadaptive techniques in addressing generally non-dispersive errors in the radar front-end. STAP will not directly address clutter internal motion effects, antenna scanning motion effects, or other hardware stability impacts to clutter cancellation performance. Radar designers need to assess the key limitations in a specific application before jumping to the conclusion that STAP will improve performance.

STAP's ability to integrate clutter cancellation (temporal) and spatial interference cancellation can be quite important to many radar systems whether they typically have to deal with intentional jamming interference or unintentional (or casual) electromagnetic interference (EMI). STAP gets away from cascaded solutions such as analog sidelobe cancellers followed by digital DPCA and/or MTI filters—that do not generally create an optimum interference cancellation solution.

Optimal Adaptive Weights (McGuffin[17]). The optimal linear estimate is determined by requiring the adapted estimation error be orthogonal to the observed vector, $\underline{r}$. Steady-state conditions are assumed in this derivation, thus the condition for orthogonality is

$$E\{\underline{r}\ \varepsilon^*\} = 0 \tag{3.24}$$

where $E\{\ \}$ is the expectation, ε is the estimation error, and * is the complex conjugate. The adaptively weighted estimate is obtained by weighting the received signal vector by the estimate of the adaptive weights:

$$\hat{s} = \underline{\hat{w}}'\ \underline{r} \tag{3.25}$$

With d defined as the desired signal (a main-beam target), the estimation error is obtained from the following equation. Then, substituting Eq. 3.25 into 3.26 and solving for the adaptive weight estimate yields the desired condition for optimal adaptive weighting:

$$\varepsilon = \hat{s} - d = \underline{\hat{w}}'\ \underline{r} - d \tag{3.26}$$

$$E\{\underline{r}(d^* - \underline{r}'\ \hat{w})\} = 0 = E\{\underline{r}\ d^*\} - \underline{R}_r\ \hat{w}$$

or

$$\hat{w} = \underline{R}_r^{-1}\ E\{\underline{r}\ d^*\} \tag{3.27}$$

where $\underline{R}_r = E\{\underline{r}\ \underline{r}'\}$. The desired signal, d, can be expressed in terms of $\underline{s}$, the signal vector of a target located in the main beam, and $\underline{b}$, the unadapted beam weight vector: $d = \underline{b}'\ \underline{s}$. This is then substituted into Eq. 3.27:

$$\hat{w} = \underline{R}_r^{-1}\ \underline{R}_s\ \underline{b} \tag{3.28}$$

Equation 3.28 is equivalent to the minimum mean square error weight equation given by Widrow,[18] which has been shown[19,20] to be the optimum set that maximizes the signal-to-interference ratio. However, complex variables are employed here rather than real variables. The interference covariance matrix is further described in terms of the individual noise, jamming, clutter, and signal contributions:

$$\underline{R}_r = N\underline{I} + \underline{K}_Z + \underline{R}_S \tag{3.29}$$

where N is receiver noise power, $\underline{K}_Z$ is the covariance matrix for clutter (temporally correlated) plus jamming (spatially correlated), and $\underline{R}_s$ is the signal covariance matrix.

Taxonomy of STAP Architectures (Ward[21]). The application of the adaptive weight equation from Eq. 3.28 in a radar system provides numerous options and complications. The options range from a fully adaptive solution across all available antenna elements and all pulses in a coherent processing interval (CPI), to reduced degrees of freedom solutions in order to be practical. The fully adaptive solution also encounters problems in the real-world where the interference environment is not well behaved (e.g., homogenous clutter). In addition, Brennan's rule[22] indicates that to achieve an adaptive solution within 3dB of the optimum answer requires $2N$ (N is the number of degrees of freedom) independent interference samples contributing to the adaptive weight estimate. With antenna array sizes in tens to hundreds of elements and CPI lengths of tens to hundreds of pulses, the number of degrees of freedom can quickly get quite large, resulting in not only fairly complex adaptive weight processing but also the more difficult problem of obtaining adequate sample support from clutter and jamming interference for a given adaptive weight solution.

As such, it is important to explore various STAP architecture options imbedded in a radar design solution. To begin, a fully adaptive array architecture is shown in Figure 3.23. This is for a linear array antenna with a distributed transmitter and digital receivers connected to each antenna element. The adaptive weight solution is developed based on at least $2 \times N \times M$ vector samples ($\underline{r}$) of length M (antenna elements) by N (pulses). The adaptive weight solution is developed and applied to the received signals from the same antenna elements and pulses of data. The adaptive weighted response is typically processed through doppler filtering (coherent integration) prior to detection processing.

Ward[21] describes the possible STAP architectures in the context of a generalized transformation matrix followed by the associated STAP processing. The four categories of STAP architectures are organized in Figure 3.24. The trades for an appropriate STAP design solution must be made in the context of the type and size of the antenna aperture under consideration, the waveforms under consideration—particularly the number of pulses per CPI—and most importantly, the interference to be cancelled (clutter and jamming). In general, for the transformation and degrees of freedom reduction to be useful, the resultant degrees of freedom must be greater than the interference rank.

Pre-Doppler, Elemental Antenna STAP. Conceptually, the simplest reduction in degrees of freedom is obtained by reducing the number of temporal degrees of

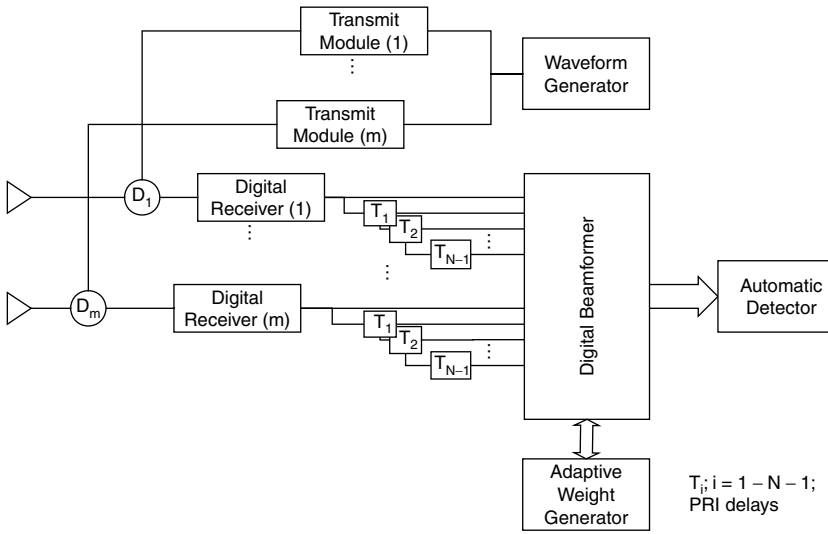

FIGURE 3.23 STAP radar block diagram

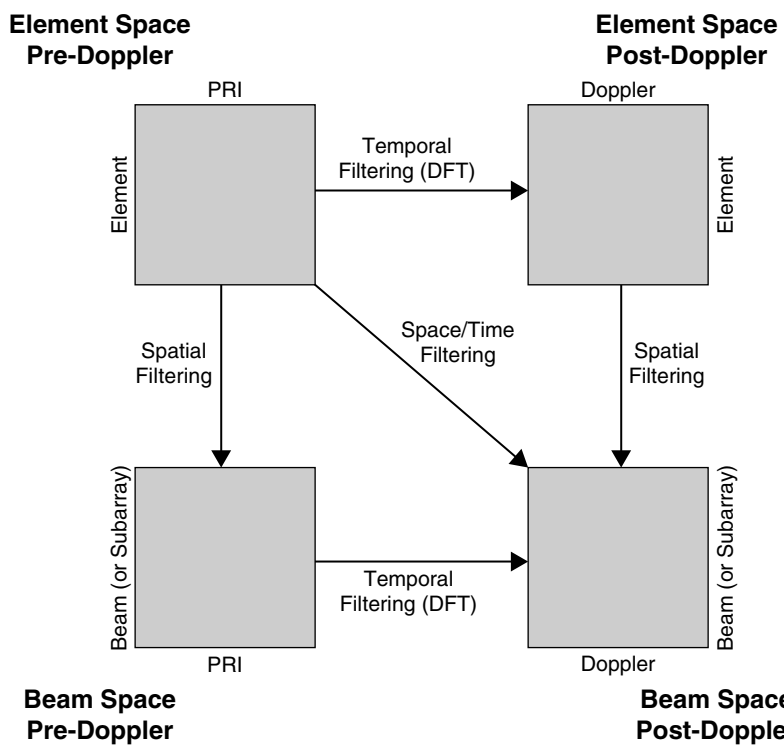

FIGURE 3.24 Reduced dimension STAP architectures

freedom in STAP while still processing the full aperture spatially. This is similar to a conventional MTI (or DPCA) architecture cascaded with doppler filtering. We call this architecture a pre-doppler, elemental-level STAP architecture. For a three-pulse version of this architecture, there are 3M degrees of freedom. In this architecture, platform motion compensation takes the general form of adjusting the antenna's phase center over the three temporally separated beams.

A basic block diagram of a radar incorporating pre-doppler, elemental-level space-time adaptive array processing is shown in Figure 3.25. An individual duplexer is placed between each transmitter's channelized output and its corresponding antenna element. Provision could be included for electronic beam steering using high-power phase shifters or transmit modules with low-power beam steering.

On receive, each duplexer output is sent to its own digital receiver. The digital receiver outputs are passed through PRI delays to yield temporally displaced data samples. A full complement of elements and time-delayed signals are sampled and used to generate the adaptive weights. Various algorithms are possible to generate the estimate of the adaptive weights from Eq. 3.28. The fairly simple Least Mean Squared algorithm generally yields fairly slow convergence rates. Other algorithms[19,23] can speed up the adaptation rate, but a more complex mechanization is required. Examples include a Recursive Least Squared algorithm, Q-R decomposition with Gram-Schmidt orthogonalization, or a Householder Transformation. The adaptive weights are then applied to the received signals and beamformed to generate three sum channel detection beams: undelayed, one-PRI delayed, and two-PRI delayed beams. These beams are, in turn, added together to form the final STAP weighted detection beam.

A simplistic view of how these three beams perform motion compensation is illustrated in Figure 3.26 for the case where the aperture is parallel with the radar's platform velocity vector. The first pulse return's phase center is advanced by aperture weighting, the second pulse return's phase center is essentially unchanged from the quiescent weights, and the third pulse return's phase center is retarded by aperture weighting. Given ideal antenna patterns, and an aperture large enough to adjust the phase centers

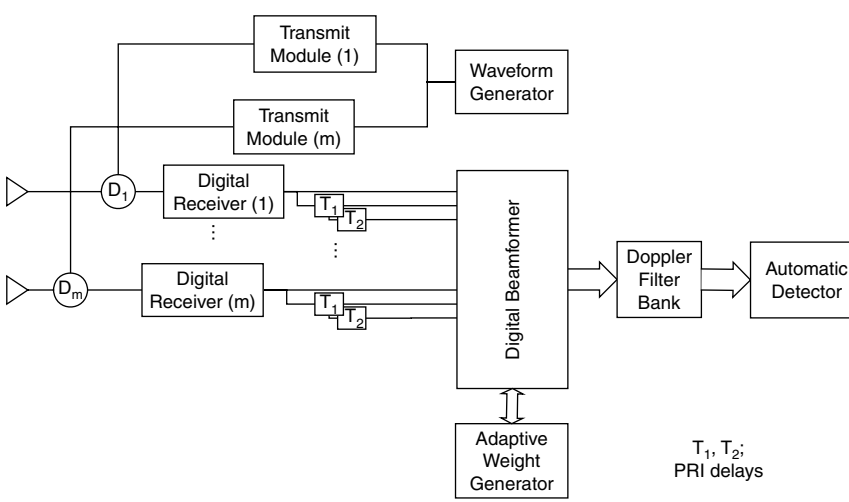

FIGURE 3.25 STAP block diagram: element space pre-doppler element space architecture

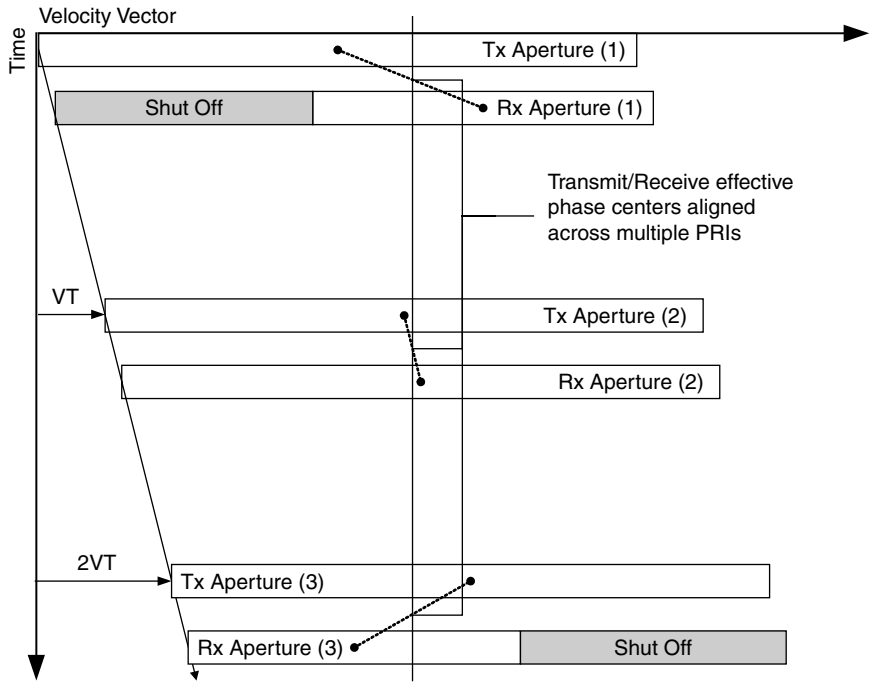

FIGURE 3.26 Aperture control for platform motion compensation

for the given platform motion, these three apertures appear as if they are stationary with respect to each other. Clutter cancellation across these three pulses is no longer limited by platform motion effects—the primary goal of platform motion compensation techniques.

Of course, this simplest condition is only illustrative, as generally the antenna elements do not behave exactly the same, and the platform motion compensation must deal with motion not only in the plane of the aperture but also orthogonal to the aperture.

Pre-Doppler, Beam-Space STAP. The first type of transformation to be considered is spatially oriented, resulting in beam-space STAP architectures. This transformation is typically required for many large apertures. The transformations can range from simple column beamforming to overlapped subarrays to beam-space transformations such as a Butler matrix. The general goal is to reduce the spatial degrees of freedom, while still providing access to array responses that allow for adequate clutter cancellation and beams that can be used to cancel directional interference as well. The resulting beam responses must span the clutter and jamming interference spatially in order for this type of transformation to be effective. For example, if a radar's clutter cancellation performance is driven by main-beam clutter residue due to platform motion effects, the beam responses must span the radar's main-beam and provide degrees of freedom to allow for motion compensation in the array main-beam. In addition, to cancel direction interference (jamming or casual EMI), the beam responses

must also span the spatial directions of that interference. An example of a simple transformation of this type would be sidelobe canceler architecture where the beam transformation would generate a sum channel main beam and select elements from the aperture as sidelobe cancellers.

Post-Doppler, Element Antenna STAP. The second type of transformation leads to what are called post-doppler STAP architectures. As the name implies, the antenna element signals are first doppler filtered and then processed through STAP. The motivation for this type of architecture is that the resultant STAP solutions can independently address a subset of the clutter interference problem isolated to clutter that remains in a single doppler filter. This technique may be more effective for radar systems where the clutter environment and waveform selection lead to unambiguous clutter returns within the radar's PRF. Two example conditions, the first with ambiguous doppler clutter and the second with unambiguous doppler clutter, are shown in Figure 3.27. The figure shows those antenna angles where the clutter doppler response remains after filtering through a single doppler filter. Figure 3.27*a* shows the response for an ambiguous PRF of 300 Hz, and Figure 3.27*b* shows the response for an unambiguous PRF of 2000 Hz for a UHF radar. This figure highlights that even with doppler processing, a given doppler filter may still include clutter returns from a number of discontiguous angular intervals. The advantages of this transformation from PRI to doppler space on overall STAP performance versus a pre-doppler architecture are more dramatic in the unambiguous doppler clutter case.

PRI-staggered doppler filter outputs are required to maintain a set of temporal degrees of freedom in this architecture. The block diagram is modified to that shown in Figure 3.28, with multiple doppler filter banks on each antenna element and PRI delay.

Post-Doppler, Beam Space STAP. The final category results from implementing both doppler and spatial transformations prior to STAP processing.

The appropriate architecture solution depends upon the radar design constraints. The number of antenna elements and beamforming requirements are key drivers in the

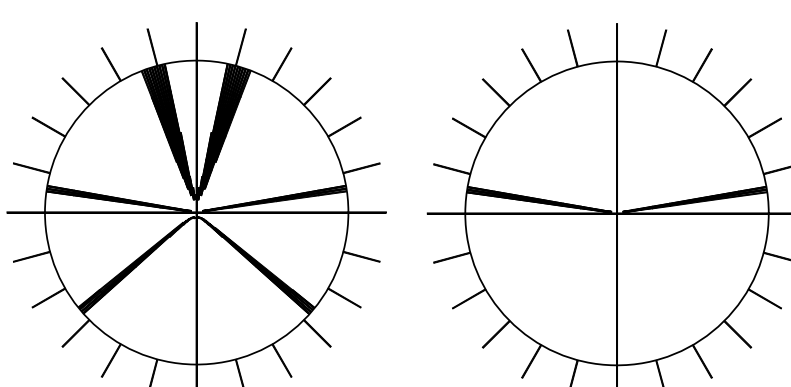

(a) UHF, low PRF (300 Hz) (b) UHF, higher PRF (2000 Hz)

FIGURE 3.27 Antenna pointing angles where clutter doppler map to a single doppler filter's passband

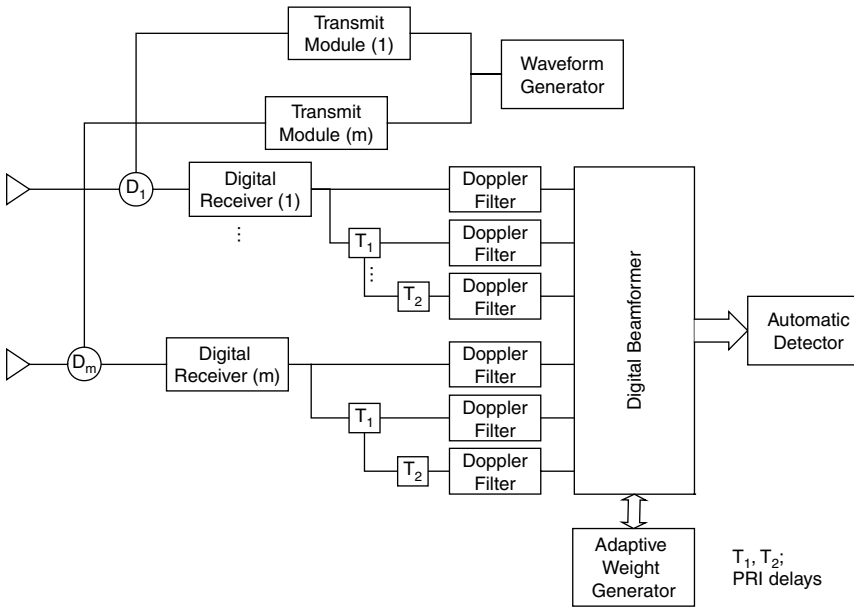

FIGURE 3.28 Element space post-doppler STAP architecture

decision whether to transform from elements to beams or subarrays. The waveforms and clutter cancellation requirements are key drivers in the decision whether to perform STAP on signals before or after doppler filtering. In addition, the overall transformation decisions to reduce degrees of freedom are driven by the interference rank for the radar problem. One caution in the design process is that if the transformation is fixed in the radar design, it is important to have excess degrees of freedom beyond the total interference rank.

Implementation Considerations. As discussed above, transformations and techniques to reduce the number of degrees of freedom in the STAP solution are important not only due to processing requirements but also because of the need for sample support on the order of two times the number of degrees of freedom for adequate STAP performance.

The basic hardware requirements for good clutter cancellation remain unchanged from conventional clutter cancellation architectures—low phase noise, low pulse jitter, etc. The requirements on the hardware may become more stringent because the STAP architecture allows the radar designer to achieve higher theoretical clutter cancellation performance levels. In addition to the above temporally based hardware requirements, there are also second-order spatially based hardware requirements. As illustrated in Figure 3.26, platform motion compensation results in different aperture weighting for successive pulses in a STAP solution. Although generally speaking, well-matched spatial channels (antenna and receiver) are driven by jamming cancellation and antenna sidelobe levels, a second-order requirement results from the need for

platform motion compensation. If antenna and receiver channels are not well matched, the resultant sum channel beams formed from different aperture illumination functions (Figure 3.26) will not be matched well enough to provide main-beam and sidelobe clutter cancellation.

Performance Comparisons. Given the number of STAP architectures and corresponding radar system design solutions, general STAP performance comparisons are difficult to come by. In general, STAP provides a robust solution to deal with clutter and jamming interference and helps alleviate hardware mismatch effects within reason (amplitude and phase adjustments are applied to antenna element and time displaced returns). Generally to address time-delay adaptive weighting, more complexity is required with a third dimension for adaptive weights—"fast-time" or returns from adjacent sampled range cells. This extension can be extremely computationally intensive and further burden the sample support problem alluded to previously.

When evaluating a radar design and trading off various waveforms and STAP processing techniques, it is important to include in the analysis key drivers such as signal bandwidth, clutter internal motion, platform motion, antenna scanning motion, the amount of sample support available from nonhomogenous and nonstationary clutter environments, and other effects such as large target samples effecting the adaptive weight solution.

3.10 EFFECT OF MULTIPLE SPECTRA

An airborne search-radar system may be operated at an altitude so that the radar horizon is approximately at the maximum range of interest. This results in sea or ground clutter being present at all ranges of interest. Other clutter sources such as rain and chaff may coexist with the surface clutter. In most instances, these sources are moving at a speed determined by the mean wind aloft and have a mean doppler frequency significantly different from that of the surface clutter. If the MTI filter is tracking the surface clutter, the spectra of the sources with a different mean doppler frequency lie in the passband of the MTI filter. A 20-kt differential in a UHF system corresponds to 30 Hz, which would generally be outside of the traditional AMTI notch filter in a 300 Hz PRF system. A single-delay secondary canceler can be cascaded with either a single-delay or a double-delay primary canceler. The primary canceler tracks the mean surface velocity and rejects surface clutter. The single-delay canceler tracks the secondary source and rejects it. Since the pass and rejection bands of the two cancelers overlap, the MTI improvement factor for each clutter source is a function of their spectral separation.

Figure 3.29 shows the improvement factor for a double canceler, which consists of two single cancelers, each tracking one of the spectra. It can be seen that as the separation varies from 0 to 1/2 of the PRF, the performance degrades from that equivalent to a double canceler to the performance of a single canceler at half of the PRF.

The triple canceler has a double-delay canceler tracking the primary spectra and a single-delay canceler tracking the secondary spectra. The performance of the primary system varies from that of a triple canceler to a level less than that of a double canceler. The secondary-system performance varies from that of a triple canceler to a performance level lower than that of a single canceler.

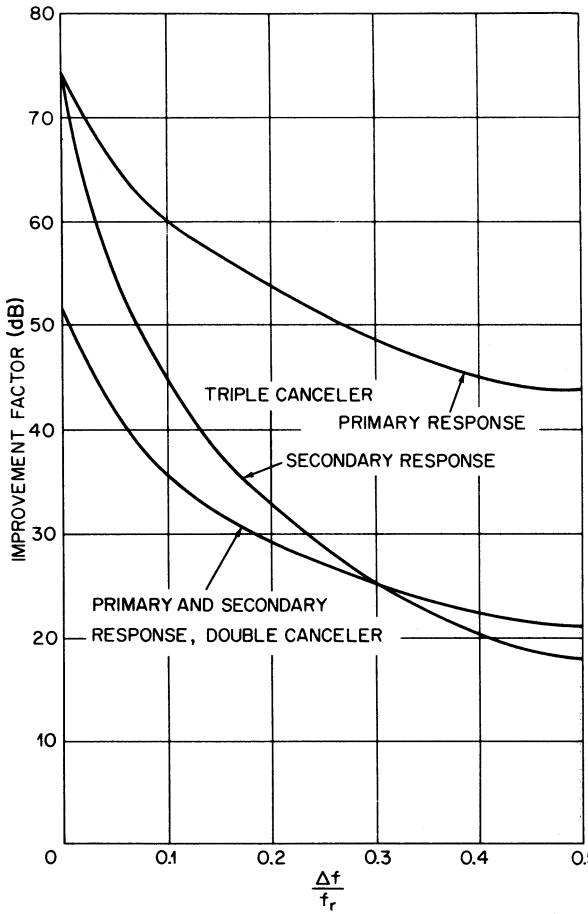

FIGURE 3.29 MTI improvement factor for a double-notch canceler tracking two spectra as a function of the normalized spectra separation $\Delta f/f_r$. Normalized spectral width $\sigma_c/f_r = 0.01$.

3.11 EXAMPLE AMTI RADAR SYSTEM

The AN/APY-9 radar, developed by Lockheed Martin for the U.S. Navy, is an example of an AMTI radar system utilized for an airborne early warning radar mission. Key features of this system include a solid-state distributed transmitter, a mechanically and electronically scanned rotating antenna, digital receivers, space-time adaptive processing, digital pulse compression, and coherent integration and auxiliary processing aimed at supporting the STAP sample selection process.

The AN/APY-9 radar addresses the AEW radar surveillance coverage requirements discussed at the beginning of this chapter, utilizing a mechanically and electronically steerable antenna located in a rotodome. There are three scanning modes of operation:

(1) mechanically scanned with an operator-selectable scan rate, (2) azimuth electronically scanned with the mechanical boresite provided as an input to the radar, and (3) mechanically scanned with additional electronic scanning within an operator-selectable azimuth region.

The transmit waveform includes TACCAR modulation to center mainbeam clutter at zero doppler frequency. However, because the radar implements adaptive clutter cancellation (STAP), the requirements on TACCAR are significantly less complex than for legacy radar systems. There is no need to include closed loop adjustments to the TACCAR modulation frequency. The optimization of the AMTI clutter cancellation filter is achieved in the STAP processing as opposed to adjusting the location of main-beam clutter to fit a fixed AMTI filter.

In order to implement STAP and electronic scanning in this radar, all 18 elements of the phased array antenna are processed on transmit and receive. The solid-state transmitter provides low-power phase shift control for electronic steering followed by power amplification in each of 18 channels. These are connected to the 18 elements of the phased array through an 18-channel rotary coupler. The transmit/receive isolation on all 18 channels is provided through circulators. The 18 channels are processed separately through 18 receivers, finally feeding the STAP subsystem with 18-digital baseband signals.

The radar performs platform motion compensation electronically as part of the STAP architecture. The radar implements an element-space pre-doppler STAP architecture. Adaptive weights are generated and applied to the 18 receive channels, forming three beams (Sum, Delta_{az}, and Omni) by weighting and summing the 18 receive channels over three pulses to provide simultaneous clutter and jamming cancellation. The adaptive weight algorithm is matched to the radar's operating parameters and is augmented with adaptive knowledge–aided sampling schemes to maximize performance in a complex, heterogeneous clutter and jamming interference environment. Doppler filtering is performed after digital beamforming.

Other functions discussed in this chapter are not required for this radar application because they do not limit performance. Examples include scanning motion compensation and multiple spectra AMTI clutter cancellation.

REFERENCES

1. R. C. Emerson, "Some pulsed doppler MTI and AMTI techniques," Rand Corporation Rept. R-274, DDC Doc. AD 65881, March 1, 1954. (Reprinted in Reference 6.)
2. T. S. George, "Fluctuations of ground clutter return in airborne radar equipment," *Proc. IEE* (London), vol. 99, pt. IV, pp. 92–99, April 1952.
3. F. R. Dickey, Jr., "Theoretical performance of airborne moving target indicators," *IRE Trans.*, vol. PGAE-8, pp. 12–23, June 1953.
4. R. S. Berkowitz (ed.), *Modern Radar: Analysis, Evaluation and System Design*, New York: John Wiley & Sons, 1966.
5. D. K. Barton, *Radar Systems Analysis*, Englewood Cliffs, NJ: Prentice-Hall, 1964.
6. D. C. Schlerer (ed.), *MTI Radar*, Norwood, MA: Artech House, Inc., 1978.
7. F. R. Dickey, Jr. and M. M. Santa "Final report on anticlutter techniques," General Electric Company Rept. R65EMH37, March 1, 1953.
8. D. B. Anderson, "A microwave technique to reduce platform motion and scanning noise in airborne moving target radar," *IRE WESCON Conv. Rec.*, vol. 2, pt. 1, 1958, pp. 202–211.

9. "Final engineering report on displaced phase center antenna," vol. 1, March 26, 1956; vols. 2 and 3, April 18, 1957, General Electric Company, Schenectady, NY.
10. H. Urkowitz, "The effect of antenna patterns on performance of dual antenna radar moving target indicators," *IEEE Trans*., vol. ANE-11, pp. 218–223, December 1964.
11. G. N. Tsandoulis, "Tolerance control in an array antenna," *Microwave J*., pp. 24–35, October 1977.
12. K. G. Shroeder, "Beam patterns for phase monopulse arrays," *Microwaves*, pp. 18–27, March 1963.
13. R. S. Grissetti, M. M. Santa, and G. M. Kirkpatrick, "Effect of internal fluctuations and scanning on clutter attenuation in MTI Radar," *IRE Trans*., vol. ANE-2, pp. 37–41, March 1955.
14. G. A. Andrews, "Airborne radar motion compensation techniques: Optimum array correction patterns," Naval Res. Lab. Rept. 7977, March 16, 1976.
15. A. R. Lopez and W. W. Ganz, "CPCT antennas for AMTI radar, vol. 2: Theoretical study," Air Force Avionics Lab. Rept. WL1630.22, AD 51858, June 1970. (Not readily available.)
16. L. E. Brennan., J. D. Mallett, and I. S. Reed, "Adaptive arrays in airborne MTI radar," *IEEE Trans*., vol. AP-24, pp. 607–615, September 1976.
17. A. L. McGuffin, "A brief assessment of adaptive antennas with emphasis on airborne radar," General Electric Company, Aircraft Equipment Division, August 1981.
18. B. Widrow and S. D. Stearns. *Adaptive Signal Processing,* New Jersey: Prentice-Hall, Inc., 1985.
19. S. P. Applebaum, "Adaptive arrays," *IEEE Trans*., vol. AP-24, pp. 585–598, September 1976.
20. L. E. Brennan, E. L. Pugh, and I. S. Reed, "Control loop noise in adaptive array antennas," *IEEE Trans*., vol. AES-7, March 1971.
21. J. Ward, "Space time adaptive processing for airborne radar," MIT Lincoln Laboratory Technical Report #1015, December. 13, 1994.
22. L. E. Brennan and F. M. Staudaher, "Subclutter visibility demonstration," Technical Report RL-TR-92-21, Adaptive Sensors Incorporated, March 1992.
23. R. A. Monzingo and T. W. Miller, *Introduction to Adaptive Arrays*, New York: John Wiley & Sons, 1980.